RSC Advances

PAPER

View Article Online
View Journal | View Issue

Cite this: *RSC Adv.*, 2021, **11**, 34842

Polyvinylpyrrolidone-assisted synthesis of highly water-stable cadmium-based metal–organic framework nanosheets for the detection of metronidazole†

Guoxu Qin,‡[ab] Duojun Cao,‡[a] Xinjun Wan,[a] Xinyun Wang[a] and Yaqiong Kong *[a]

Recently, much effort has been dedicated to ultra-thin two-dimensional metal–organic framework (2D MOF) nanosheets due to their outstanding properties, such as ultra-thin morphology, large specific surface area, abundant modifiable active sites, *etc.* However, the preparation of high-quality 2D MOF nanosheets in good yields still remains a huge challenge. Herein, we report 2D cadmium-based metal–organic framework (Cd-MOF) nanosheets prepared in a one-pot polyvinylpyrrolidone (PVP)-assisted synthesis method with high yield. The Cd-MOF nanosheets were characterized with good stability and dispersion in aqueous systems, and were highly selective and sensitive to the antibiotic metronidazole (MNZ) with low limit of detection (LOD: 0.10 μM), thus providing a new and promising fluorescent sensor for rapid detection of MNZ in aqueous solution.

Received 12th July 2021
Accepted 20th October 2021

DOI: 10.1039/d1ra05349c

rsc.li/rsc-advances

1. Introduction

Nowadays, antibiotics are extensively utilized for combating protozoa and infectious bacteria to improve the health of mankind and livestock due to their powerful antibacterial activity.[1–3] However, it was reported recently that antibiotics had imposed a great negative impact on the earth in different environmental matrices even at very low levels because of the indiscriminate usage and difficult degradation. And now antibiotics have been classified as emerging contaminants.[4,5] Of these antibiotics, metronidazole (MNZ) is generally used in the treatment of anaerobic bacteria and parasites[6] and also added in poultry feed to promote weight gain.[7] But over-accumulated MNZ in human tissue may trigger a variety of diseases like peripheral nephropathy and ataxia,[8] and excessive MNZ in aquatic environments can pose potential risks for other organisms.[9] Therefore, the establishment of effective and accurate determination method of MNZ is extremely necessary.

To date, validated analytical methods have been developed to detect the MNZ in different matrices, including ultra-performance liquid chromatography mass spectrometry,[10] fluorescent carbon dots,[11,12] electrochemical sensor,[13] immunoassay[14] and aptamer-based biosensor.[15] However, these methods require either advanced equipment, or high cost and complicated sample processing. Regarding the drawbacks above mentioned methods, exploiting an alternative facile method with high selectivity, good recognition capability and rapid response for MNZ is significant importance.

As an emerging molecular crystal porous material, metal–organic framework (MOF) can be designed and synthesized by selecting appropriate metal-containing nodes and organic ligands.[16] Fluorescent MOFs have been proven as a promising method of constructing sensors due to their specific structures, excellent porosity and active sites.[17] However, large amounts of fluorescent MOF sensors only concentrated on the preparation of micron-sized three-dimensional (3D) MOF crystals and lost sight of their better properties.[18] Recently, the 2D MOF nanosheets, which combine the advantages of MOF and 2D materials, have been extensively reported in various fields, such as catalysis,[19] gas separation,[20] supercapacitors,[21] biomimetic enzymes,[22] sensing,[23,24] *etc.* Especially, 2D MOF nanosheets are remarkably attractive platform candidates for signal transduction through fluorescence resonance energy transfer or photoinduced electron-transfer pathway because of their ultra-thin thickness and large surface area with highly accessible active sites, which is beneficial to the response speed and sensitivity.[25] Of late, some studies about fluorescent sensors based on 2D MOF nanosheets have been published. For example, Sun's team recently reported a single-layered sulfur-rich 2D MOF nanosheets 2D-NCS($\{[Co(NCS)_2(pyz)_2]\}_{6n}$) (pyz = pyrazine) which serves as an ideal adsorbent materials for capturing $HgCl_2$ from aqueous solution with the maximum uptake capacity of 1698 mg g^{-1}.[26] Ying *et al.*, prepared a scalable 2D MOF nanosheets ($Cu(bpy)_2(OTf)_2$, bpy =

[a]*Engineering Technology Center of Department of Education of Anhui Province, Institute of Novel Functional Materials and Fine Chemicals, College of Chemistry and Materials Engineering, Chaohu University, Chaohu 238024, P. R. China. E-mail: xiayaqun0718@163.com*

[b]*College of Chemistry and Materials Science, Anhui Normal University, 189 Jiuhua Southern Road, Wuhu, 241002, P.R. China. E-mail:*

† Electronic supplementary information (ESI) available. See DOI: 10.1039/d1ra05349c

‡ These authors contributed equally to this work.

4,4-bipyridine, OTf = trifluoromethanesulfonate) using a novel shear exfoliation method, whose thickness is 3–5 nm. The sensor was able to monitor superoxide anion released from cancer cells with excellent sensitivity, flexibility and stability.[27] Wei's group employed a phosphates-responsive 2D MOF nanozymes (Zn-TCPP(Fe)) to develop a colorimetric alkaline phosphatase (ALP) activity assay, which not only detected ALP, but also exhibited broad applications for evaluating the ALP enzyme inhibitor.[28] Toward this end, it is of far-reaching significance to construct well-defined 2D ultra-thin MOF sensors using novel strategies for environmental protection and bio-medical treatment.

However, it is still a great challenge to efficiently synthesize highly stable 2D MOF nanosheets. Recently, a facile polymer or surfactant-assisted synthetic method for the preparation of a series of 2D MOF nanosheets was developed, such as polyvinylpyrrolidone (PVP),[29–32] cetyltrimethylammonium bromide (CTAB),[33] sodium dodecyl benzene sulfonate (SDBS)[34] and sodium dodecyl sulfate (SDS).[35] In the method, they mainly play two important roles. Firstly, they limit the stacking of MOF layers along the vertical direction, which is conducive to the formation of ultrathin MOF nanosheets. Secondly, they prevent the aggregation of synthesized MOF nanosheets and stabilize them.

Herein, we have prepared a 2D cadmium-based metal–organic framework (Cd-MOF) nanosheets in one-pot PVP-assisted synthesis method with high yield. The purpose of adding surfactants is to control the crystal growth and promote the formation of special morphologies.[36] Although the bulk Cd-MOF was reported previously,[37] the 2D Cd-MOF nanosheet was obtained for the first time *via* using PVP-assisted method. The nanosheets exhibited good stability and dispersibility in aqueous system. Most importantly, Cd-MOF nanosheets performed superior metronidazole (MNZ) sensing properties over other antibiotics, thus encouraging us to employ the MOF nanosheets to determinate MNZ in domestic water samples.

2. Experimental section

2.1 Materials and analytical instruments

All chemical reagents were analytically pure and used directly without further purification. Hexahydrate and cadmium nitrate ($Cd(NO_3)_2\cdot 6H_2O$), 1,10-phenanthroline (Phen), benzene-1,4-dicarboxylic acid (H_2BDC), PVP K30, gentamicin (GEN), kanamycin (KAN), penicillin (PEN), amoxicillin (AMX), cefixime (CFX) cefradine (CED), roxithromycin (ROX), azithromycin (AZM), nitrofurantoin (NIT), doxycycline hyclate (DYC) and metronidazole (MNZ) were all obtained from Sinopharm Chemical Reagent Co. Ltd(Shanghai, China). Deionized water (18.2 MΩ cm) was prepared by a Millipore water purification system.

Powder X-ray diffraction (PXRD) patterns were measured by a Shimadzu XRD-6000 X-ray diffractometer (Japan) using Cu Kα radiation (40 kV, 20 mA, 0.02° s^{-1}, from 5° to 50°) at room temperature. Scanning electron microscopy (SEM) images of the final product were taken on a COXEM scanning electron microscope (Korea), employing the accelerating voltage of 5 kV. Transmission electron microscopy (TEM) images of Cd-MOF nanosheets were obtained on a JEOL-2011 transmission electron microscope (Japan) with an accelerating voltage of 200 kV. The UV-vis spectra were monitored on a Metash 6100 UV-vis spectrophotometer (China). The fluorescence lifetime and quantum yield were measured on a full-functional steady/transient FLs980 fluorescence spectrophotometer (Edinburgh, UK). Fluorescent spectra were measured on an FLSP 920 fluorescence spectrophotometer (China), using the photomultiplier tube voltage of 700 V, the excitation and emission slit widths of 5 nm.

2.2 Synthesis bulk Cd-MOF

In a typical experiment, a mixture of $Cd(NO_3)_2\cdot 6H_2O$ (0.309 g), Phen (0.083 g) and H_2BDC (0.090 g) were added into a 24.0 mL mixed solvent of deionized water and acetonitrile (v/v, 5/1) at room temperature. After stirring for 10 min, the mixture was sealed in a 50 mL Teflon-lined stainless reactor and heated at 120 °C for 12 h under autogenous pressure, and then cooled to room temperature. Colorless crystals were obtained and washed 3 times with distilled water and ethanol, respectively, and finally dried in air at 65 °C for 14 h.

2.3 Surfactant-assisted synthesis Cd-MOF nanosheets

For comparison with bulk Cd-MOF, nanosheets were prepared in the similar way, except that 0.05 g PVP (K30) was added. Finally, Cd-MOF nanosheets were washed with ethanol and collected by centrifuging at 10 000 rpm for 20 min and dried at 70 °C for 14 h.

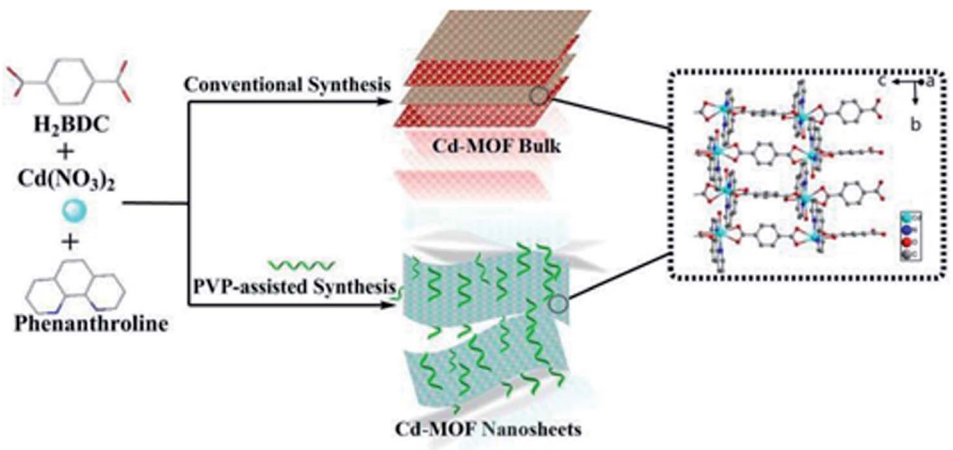

Scheme 1 The synthesis of Cd-MOF *via* conventional and PVP-assisted methods.

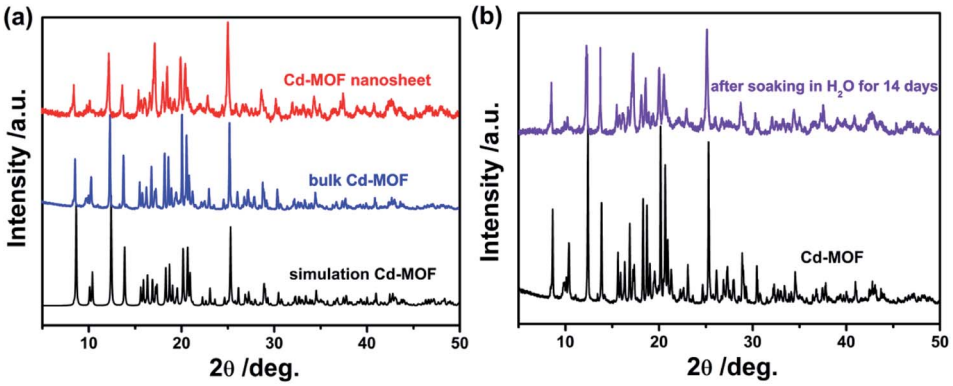

Fig. 1 (a) XRD pattern of the simulated Cd-MOF, the product Cd-MOF and Cd-MOF nanosheets; (b) XRD pattern of the product Cd-MOF and after soaking in water for 14 days.

The yield of the product is 53%. The preparation process of bulk and Cd-MOF nanosheets was shown in Scheme 1. 2 mg of above white powder was suspended in 20.0 mL of EtOH and sonicated for 1 h. After centrifugation for 3000 rpm, the upper colloidal suspension was collected for TEM characterization.

2.4 Photoluminescence based detection measurements

Before fluorescent tests, 2D Cd-MOF nanosheets colloidal suspension was obtained through dispersing 10 mg Cd-MOF nanosheets into 20 mL deionized water, sonicating for 1 h and centrifuging for 3000 rpm to collected the upper colloidal suspension. And 2 mg mL^{-1} bulk Cd-MOF suspension prepared by dispersing proper amounts of the bulk Cd-MOF into deionized water.

In a typical measurement, the above upper colloidal suspension of the 2D Cd-MOF nanosheets were used for photoluminescence sensing experiments. In order to explore the selectivity and sensitivity of the 2D Cd-MOF nanosheets toward some common antibiotics, 2×10^{-4} M various antibiotic aqueous solutions as stock solutions were separately prepared, including aminoglycoside (GEN, KAN), β-lactams (PEN, AMX; CFX, CED), macrolide (ROX, AZM), nitrofurans (NIT), tetracyclines (DYC) and metronidazole (MNZ). During experiments, 1 mL of antibiotic solution was instilled into 1 mL of the above upper colloidal suspension. After mixing thoroughly at room temperature by stirring, the fluorescence spectrum of the system was recorded immediately with the excitation at 296 nm and emission wavelength in the range from 320 to 570 nm. For comparison, the bulk Cd-MOF was also subjected the similar fluorescence sensing test.

3. Results and discussion

3.1 Structural characterization and morphology

Fig. 1a displayed the PXRD patterns of the obtained bulk Cd-MOF and Cd-MOF nanosheets. The PXRD analyses of prepared Cd-MOF revealed that patterns of experimental products and simulated crystal phase matched very well (Cambridge Crystallographic Data Centre (CCDC): 695680),[37] confirming the successful formation of Cd-MOF. In addition, the peaks of Cd-MOF nanosheets were broad than that of bulk Cd-MOF, indicating the crystallinity of Cd-MOF nanosheets was poor. Furthermore, after being immersed in H_2O for 14 days, the measured PXRD patterns were almost identical to those of the original sample (Fig. 1b), demonstrating its excellent stability in water. The morphology of obtained products was characterized by SEM. As shown in Fig. 2a, bulk Cd-MOF is a block with a width of 10–20 μm. On magnification, it can be found that these large blocks were layered (Fig. 2b). PVP assisted synthesis of Cd-MOF nanosheets showed hierarchically stacking lamellae with interspace (Fig. 2c) and the average thickness of 2D sheets is about 20 nm around. The results for morphologies and particle sizes of Cd-MOF could be attributed to the effect of the surfactants, where PVP acted as a capping agent to block the growth of crystalline particles and the growth processes could be quenched at an early stage.[38] The TEM image of the Cd-MOF nanosheets after ultrasonic treatment was shown in Fig. 2d. It could also be seen from the figure that the thinner nanosheets were obtained after ultrasonic treatment. Besides, The Tyndall

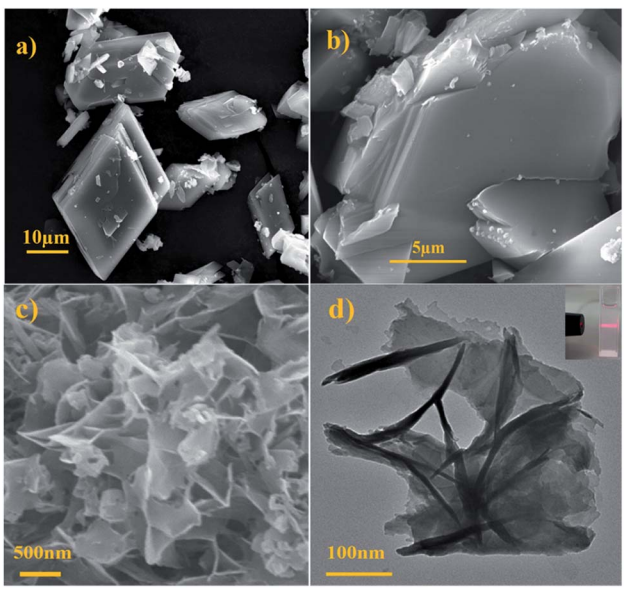

Fig. 2 (a and b) SEM images of the as-obtained bulk product; (c and d) SEM and TEM images of nanosheet product. Inset: Tyndall effect of the nanosheet product.

effect of nanosheets was obviously observed in the aqueous system (Fig. 2d, inset).

3.2 Optical properties

The fluorescence properties of Phen, H_2BDC and Cd-MOF were systematically investigated. As shown in Fig. 3, the emission spectrum of Phen solution excited at 299 nm shows a broad band peaked at 367 nm. Compared to linker Phen, the Cd-MOF exhibits an emission band at 365 nm when excited at 301 nm with the quantum yield of 12.7%, while the fluorescence intensity of the H_2BDC ligand is almost zero. Therefore, the luminescence of Cd-MOF primarily originates from ligand Phen. And Cd-MOF displays more significant fluorescence intensity than the free ligand Phen. This may be attributed to the unique coordination of the central Cd^{2+} ions with the organic ligands, which increases the rigidity of the ligand conformation, thereby reducing the radioactive decay of the excited state in the ligand.[39]

3.3 Stability of Cd-MOF suspended in aqueous system

The luminescent stability of Cd-MOF nanosheet colloidal suspension in aqueous solution was also investigated and the results were performed in inset of Fig. 3. According to fluorescent spectra, the intensity of Cd-MOF colloidal suspension underwent no significant optical changes over a period of one month, proving that nanosheet colloidal was in good compatibility with aqueous medium.

3.4 Sensing of antibiotics in aqueous solution

Based on the good dispersion in aqueous system, the selective recognition of Cd-MOF nanosheets toward different antibiotics were also evaluated. As can be seen from Fig. 4, when nanosheet colloidal suspension was treated with same volume different antibiotics, the fluorescence of Cd-MOF nanosheets was quenched in different degrees. Markedly, KAN, GEN, CED, AZM, ROX, PEN only have slight influence on the fluorescence of Cd-MOF nanosheet; and AMX, CFX, NIT, DYC can partly quench the fluorescence of Cd-MOF nanosheet. Comparatively, MNZ can strongly quench the fluorescence of as-obtained fluorescent matter, which was almost no emission excited at 301 nm. The bar graph could further clearly illustrated that Cd-MOF nanosheets displayed excellent response for antibiotic MNZ (Fig. S1†). Moreover, the time of Cd-MOF nanosheets sensing for MNZ was very short as fast as 20 seconds. And the fluorescence of Cd-MOF nanosheets was dramatically quenched when combining with MNZ (Fig. 5a). To ensure anti-interference of Cd-MOF nanosheets toward MNZ, the competition experiment was further implemented. As expect, it could be seen that MNZ still have outstanding quenching effects among other antibiotics, indicating that the nanosheets might be used as a promising probe for MNZ with high selectivity (Fig. 5b).

Upon gradual addition of MNZ, the emission intensity of Cd-MOF decreased gradually. More notably, when the concentration reached 62 μM, fluorescence nearly vanished (Fig. 6a). From inset of Fig. 6b, there was a good linear relationship between Cd-MOF nanosheets and MNZ ($R^2 = 0.997$) in low concentration range. Based on Stern–Volmer equation: $I_0/I = 1 + K_{sv}[C]$, and LOD $= 3SD/K_{sv}$, the limit of detection (LOD) and quenching constant (K_{sv}) were calculated to be 0.10 μM and 1.56 $\times 10^5$ M^{-1}, respectively. Analogously, on account of the fluorescent titration curve of bulk Cd-MOF toward MNZ (Fig. S2†), however, when the concentration of MNZ reached 340 μM, the fluorescence of the matter can be strongly quenched. According to the inset of Fig. S3,† the LOD and K_{sv} of bulk Cd-MOF were 1.3 μM and 2.63 $\times 10^4$ M^{-1}. In comparison, LOD of Cd-MOF nanosheets was about 10 folds lower than that of bulk Cd-MOF while the K_{sv} of bulk Cd-MOF was about 6 folds higher than the counterpart of Cd-MOF nanosheets, illustrating that the detection performance of Cd-MOF nanosheets sensing for MNZ was superior over that of bulk Cd-MOF. Compared with some fluorescence sensing materials reported in the literature, the present Cd-MOF nanosheets displays better detection limit (see Table 1).

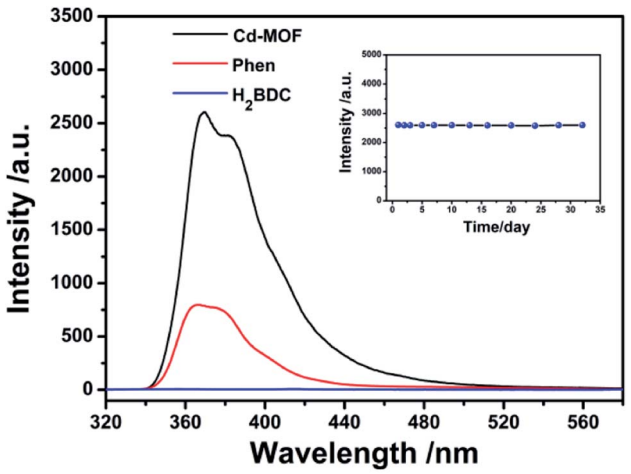

Fig. 3 The fluorescent spectra of Cd-MOFs colloidal suspended (black), Phen (red) and H_2BDC (blue) at room temperature. The inset is the fluorescence stability test of Cd-MOF colloidal suspended in aqueous systems (excited at 301 nm).

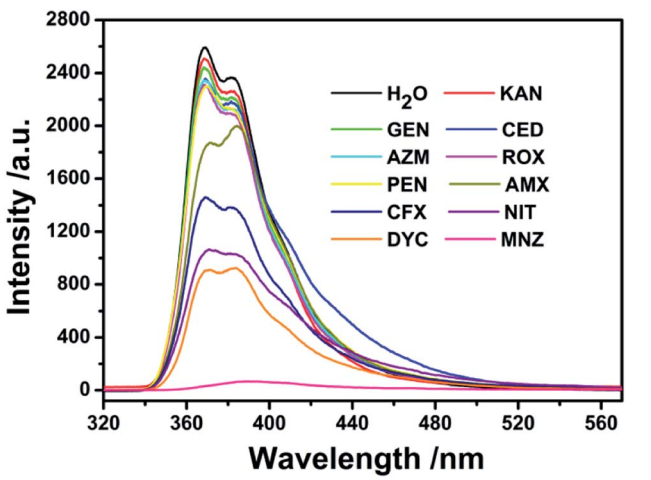

Fig. 4 The fluorescence spectra of Cd-MOF colloidal suspended toward various antibiotics (200 μM) in aqueous solution (excited at 301 nm).

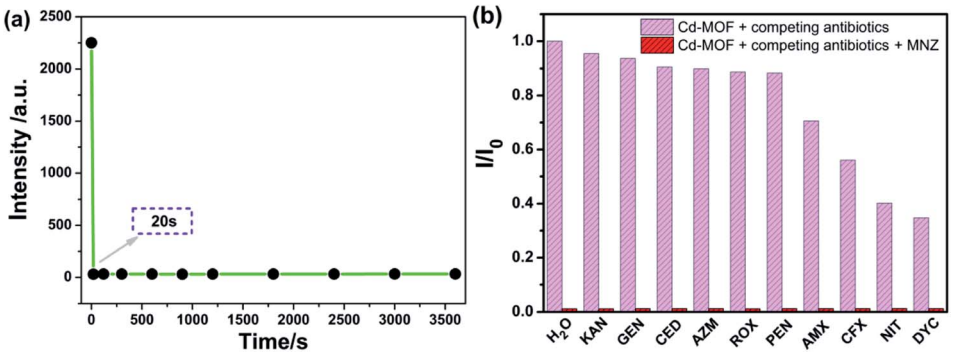

Fig. 5 (a) The response time of Cd-MOF nanosheets toward MNZ; (b) fluorescence intensity ratio (I/I_0) of Cd-MOF colloidal suspension, magenta bars: adding competing antibiotics, red bars: adding competing antibiotics and MNZ, I_0 represents intensity of Cd-MOF nanosheets in water solution, I represents intensity of Cd-MOF nanosheets with antibiotics (excited at 301 nm).

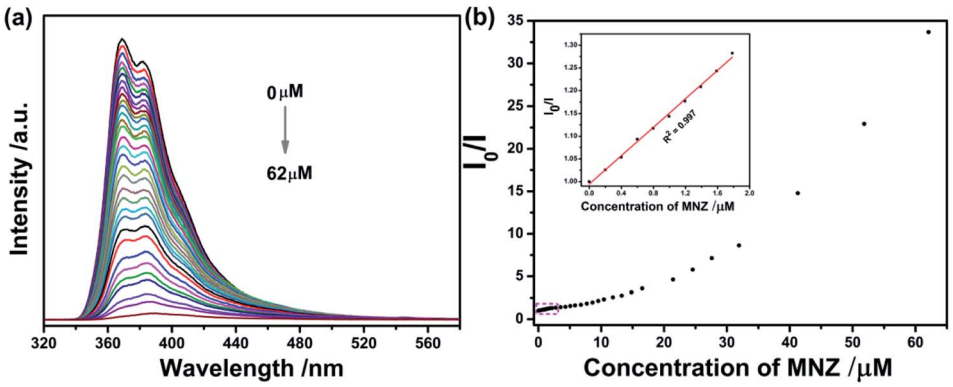

Fig. 6 (a) Concentration-dependent fluorescence spectra of Cd-MOF nanosheets with various concentrations of fluoride. (b) The correlation curve between the fluorescence intensity ratio (I_0/I) of Cd-MOF nanosheets and the concentration of MNZ, inset: the corresponding linear relation in the low concentration region.

3.5 Fluorescence quenching mechanism to MNZ

It has been well known that causing the luminescence quenching behavior includes three significant factors: structural changes of the sensors, photo-induced electron transfer and energy transfer.[50] From this, the underlying quenching mechanism of Cd-MOF sensor for MNZ was discovered. As mentioned before, Cd-MOF nanosheets displayed good water-stability for over a month with no fluorescence intensity weakening, implying there was no apparent structure changes. Besides, the PXRD patterns (Fig. 7a) also showed no structure collapse occurred when Cd-MOF was treated with MNZ in aqueous system. Photoinduced electron transfer was another possible sensing mechanism. Fig. 7b presented the HOMO and LUMO energy levels of different antibiotics and ligands (Phen and H_2BDC) through the density functional theory (DFT) calculation. It was obviously observed that CFX and NIT had lower LUMO energy level than Phen, which explained the reason of luminescent quenching of CFX and NIT. However, the antibiotic MNZ possessed higher LUMO energy level than ligands Phen and H_2BDC, indicating that the process of excited-state electrons transferring from framework to MNZ is almost impossible. Thus, to further investigate the quenching mechanism, the excitation spectrum of Cd-MOF and the UV-visible absorption spectra of detected antibiotics were obtained. As presented in Fig. S4,† the absorption peak of MNZ shared maximum degree of overlapping (located at 270–360 nm) with the excitation peak of Cd-MOF. This fact suggests that the excitation energy of Cd-MOF is nearly absorbed by MNZ. That is to say, the existence of inner filter effect (IFE) between

Table 1 Comparison of some fluorescent materials for sensing metronidazole

Fluorescent matter	K_{sv}/M^{-1}	LOD/μM	Reference
$[Ln_2(2,3'\text{-oba})_3(phen)_2]_n$	5.06×10^4	16	40
$[Zn_2(oba)_4(4,4'\text{-bpy})_2]_n$	6.44×10^3	4.7	41
$[Zn_4O(BCTPE)_3]$	5.98×10^4	3.5	42
$[In(dtztp)_{0.5}(OH)(H_2O)]H_2O$	9.04×10^4	29	43
$Pb_{1.5}(DBPT)_2 \cdot (DMF)_3(H_2O)_4$	7.3×10^4	52	44
$[Cd_3(DBPT)_2(H_2O)_4] \cdot 5H_2O$	8.0×10^4	58	45
Tb-MOF	1.1×10^5	0.70	46
$Eu_2(dtztp)(OH)_2(DMF)(H_2O) \cdot 2H_2O$	1.80×10^4	76	47
$\{Eu_2(TDC)_3(CH_3OH)_2 \cdot (CH_3OH)\}_n$	7.5×10^4	2.0	48
$[Eu_2(2,3'\text{-oba})_3(phen)_2]_n$	4.93×10^4	10	49
2D Cd-MOF nanosheets	1.56×10^5	0.10	This work

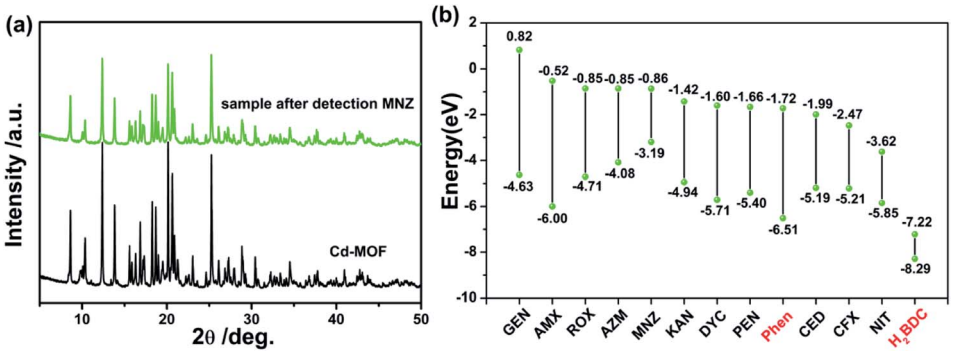

Fig. 7 (a) XRD patterns of Cd-MOF without/with MNZ; (b) HOMO–LUMO energy levels and molecular Frontier orbital energy-level diagram of each antibiotic, ligand of Phen and H_2BDC.

Cd-MOF and MNZ leads to the fluorescence quenching.[51,52] Meanwhile, as shown in Fig. S4,† there were partial overlap between the excitation peak of Cd-MOF nanosheet and the absorption spectrum of AMX, CFX, NIT and DYC, which explained that the above four antibiotics can quench Cd-MOF to a certain degree.

To further confirm the type of quenching, the fluorescence lifetimes of Cd-MOF nanosheets were determined. The average fluorescence lifetime of Cd-MOF nanosheets was 1.43 ns (Fig. S5†). Moreover, according to the formula associated with dynamic quenching, $K_{sv} = K_q\tau_0$,[53] where K_q is the quenching rate constant and τ_0 is the fluorescence lifetime of Cd-MOF nanosheets. The calculated K_q is 1.43×10^{15} M^{-1} s^{-1} less than 1.0×10^{10} M^{-1} s^{-1}, suggesting static quenching rather than dynamic quenching in the process of detection.[54,55] Therefore, static quenching may mainly be involved in the fluorescence quenching of Cd-MOF nanosheets, and it is further demonstrated that IFE of MNZ is the primary reason for the fluorescence quenching of Cd-MOF nanosheets.

3.6 Detection of MNZ in real samples

To verify the practical application of the 2D Cd-MOF nanosheets sensing for MNZ, the Chaohu Lake water (natural water) and the tap water with MNZ spiked at the concentration ranges of 0–1.5 μM were separately used as real water samples. Furthermore, based on the medicine consideration of MNZ, urine was also chosen as real case. The related results are list in Table 2. The recovery rate of MNZ in Chaohu Lake water, tap water and urine was 99.3–101.3%, 98.5–99.2% and 98.8–102.2%, respectively. The corresponding deviation (RSD) was less than 5.4%, 5.2% and 5.8%, respectively. The above experimental results indicate that the as-obtained Cd-MOF nanosheet is promising for the detection of MNZ in practical examples.

Table 2 Analytical results (mean ± σ, $n = 3$) for the determination of MNZ in real samples

Sample	Spiked/μM	Measured/μM	Recovery/%	RSD ($n = 3$, %)
Tap water	0	Not detected		
	0.50	0.49	98.5	5.2
	1.00	1.04	99.1	4.0
	1.50	1.49	99.2	3.3
Chaohu Lake water	0	Not detected		
	0.50	0.50	100.1	5.4
	1.00	0.99	99.3	4.6
	1.50	1.52	101.3	4.6
Urine	0	Not detected		
	0.50	0.51	98.8	5.8
	1.00	1.02	102.2	4.4
	1.50	1.49	100.4	4.8

4. Conclusion

In summary, new 2D Cd-MOF nanosheets have been successfully prepared in the mixed system of water/MeCN/PVP, which was confirmed by PXRD. The Cd-MOF nanosheets displayed excellent dispersion and high stability in aqueous solution. Satisfactorily, the Cd-MOF also showed high selectivity and sensitivity for antibiotic MNZ with distinct fluorescence intensity change in aqueous solution, whose limit of detection was as low as 0.10 μM. Therefore, it could be concluded that the novel 2D Cd-MOF nanosheets might be used as a potential sensor for MNZ in aqueous medium.

Conflicts of interest

There are no conflicts to declare.

Acknowledgements

This work was financially supported by the Natural Science Foundation of Anhui Higher Education Institutions [Grant Number KJ2020A0677], and Natural Science Foundation of Chaohu University [Grant Number XLZ-202007; XLY-202002]. Y. Q. Kong would like to thank Chaohu University for the Start-Up grant (Grant Number KYQD-202006).

References

1 Y. Q. Zhang, X. H. Wu, S. Mao, W. Q. Tao and Z. Li, *Talanta*, 2019, **204**, 344–352.

2 N. Das, J. Madhavan, A. Selvi and D. Das, *3 Biotech*, 2019, **9**, 231.
3 G. Reichert, S. Hilgert and S. Fuchs, *Environ. Pollut.*, 2019, **255**, 113140.
4 H. Eskandari, M. Amirzehni, H. Asadollahzadeh, J. Hassanzadeh and P. A. Eslami, *Sens. Actuators, B*, 2018, **275**, 145–154.
5 B. Wang and B. Yan, *Talanta*, 2020, **208**, 120438.
6 D. Leitsch, *Parasitology*, 2019, **146**, 1167–1178.
7 H. B. Ammar, M. B. Brahim, R. Abdelhedi and Y. Samet, *Mater. Sci. Eng. C*, 2016, **59**, 604–610.
8 Y. Liu, J. Liu, H. Tang, J. Liu, B. Xu, F. Yu and Y. Li, *Sens. Actuators, B*, 2015, **206**, 647–652.
9 W. Liu, J. Zhang, C. Li, L. Tang, Z. Zhang and M. Yang, *Talanta*, 2013, **104**, 204–211.
10 S. L. Stancil, L. Haandel, S. Abdel-Rahman and R. E. Pearce, *J. Chromatogr. B: Anal. Technol. Biomed. Life Sci.*, 2018, **1092**, 272–278.
11 J. Tang, Y. Zhang, Y. Liu, D. Liu, H. Qin and N. Lian, *RSC Adv.*, 2019, **9**, 38174–38182.
12 S. Yang, L. Wang, L. Zuo, C. Zhao, H. Li and L. Ding, *Microchim. Acta*, 2019, **186**, 652.
13 N. Xiao, J. Deng, J. Cheng, S. Ju, H. Zhao, J. Xie, D. Qian and J. He, *Biosens. Bioelectron.*, 2016, **81**, 54–60.
14 C. S. Thompson, I. M. Traynor, T. L. Fodey and S. R. H. Crooks, *Anal. Chim. Acta*, 2009, **637**, 259–264.
15 H. Wei, R. Cai, H. Yue, Y. Tian and N. Zhou, *Anal. Chim. Acta*, 2020, **1128**, 203–210.
16 Y. Yan, A. E. O'Connor, G. Kanthasamy, G. Atkinson, D. R. Allan, A. J. Blake and M. Schroder, *J. Am. Chem. Soc.*, 2018, **140**, 3952–3958.
17 H. Yin and X. Yin, *Acc. Chem. Res.*, 2020, **53**, 485–495.
18 Q. Liu, X. Li, Y. Wen, Q. Xu, X. T. Wu and Q. L. Zhu, *Adv. Mater. Interfaces*, 2020, **7**, 2000813.
19 M. Zhong, S. Zhang, A. Dong, Z. Sui, L. Feng and Q. Chen, *J. Mater. Sci.*, 2020, **55**, 10388–10398.
20 J. M. Hou, Y. Y. Wei, S. Zhou, Y. J. Wang and H. H. Wang, *Chem. Eng. Sci.*, 2018, **182**, 180–188.
21 Z. X. Li, B. L. Yang, K. Y. Zou, L. Kong, M. L. Yue and H. H. Duan, *Carbon*, 2019, **144**, 540–548.
22 W. Bai, S. Li, J. Ma, W. Cao and J. Zheng, *J. Mater. Chem. A*, 2019, **7**, 9086–9098.
23 L. J. Han, D. Zheng, S. G. Chen, H. G. Zheng and J. Ma, *Small*, 2018, **14**, e1703873.
24 G. Qin, J. Wang, L. Li, F. Yuan, Q. Zha, W. Bai and Y. Ni, *Talanta*, 2021, **221**, 121421.
25 D. Ning, Q. Liu, Q. Wang, X. M. Du, W. J. Ruan and Y. Li, *Sens. Actuators, B*, 2019, **282**, 443–448.
26 C. Wang, C. He, Y. H. Luo, S. Su, J. Y. Wang, D. L. Hong, X. T. He, C. Chen and B. W. Sun, *Chem. Eng. J.*, 2020, **379**, 122337.
27 Q. Qiu, H. Chen, Z. You, Y. Feng, X. Wang, Y. Wang and Y. Ying, *ACS Appl. Mater. Interfaces*, 2020, **12**, 5429–5436.
28 X. Wang, X. Jiang and H. Wei, *J. Mater. Chem. B*, 2020, **8**, 6905–6911.
29 M. Zhao, Y. Wang, Q. Ma, Y. Huang, X. Zhang, J. Ping, Z. Zhang, Q. Lu, Y. Yu, H. Xu, Y. Zhao and H. Zhang, *Adv. Mater.*, 2015, **27**, 7372–7378.
30 G. Zhan and H. C. Zeng, *Adv. Funct. Mater.*, 2016, **26**, 3268–3281.
31 L. He, F. Duan, Y. Song, C. Guo, H. Zhao, J.-Y. Tian, Z. Zhang, C.-S. Liu, X. Zhang, P. Wang, M. Du and S.-M. Fang, *2D Mater.*, 2017, **4**, 025098.
32 C. Kutzscher, A. Gelbert, S. Ehrling, C. Schenk, I. Senkovska and S. Kaskel, *Dalton Trans.*, 2017, **46**, 16480–16484.
33 A. Pustovarenko, M. G. Goesten, S. Sachdeva, M. Shan, Z. Amghouz, Y. Belmabkhout, A. Dikhtiarenko, T. Rodenas, D. Keskin, I. K. Voets, B. M. Weckhuysen, M. Eddaoudi, L. de Smet, E. J. R. Sudhölter, F. Kapteijn, B. Seoane and J. Gascon, *Adv. Mater.*, 2018, **30**, 1707234.
34 X. Gao, R. Cui, M. Zhang and Z. Liu, *Mater. Lett.*, 2017, **197**, 217–220.
35 H. Fan, H. Yu, X. Wu, Y. Zhang, Z. Luo, H. Wang, Y. Guo, S. Madhavi and Q. Yan, *ACS Appl. Mater. Interfaces*, 2016, **8**, 25261–25267.
36 X. Sang, D. Liu, J. Song, C. Wang, X. Nie, G. Shi, X. Xia, C. Ni and D. Wang, *Ultrason. Sonochem.*, 2021, **72**, 105461.
37 Z. Wang, W. Han and Z. Liu, *Acta Crystallogr., Sect. E: Struct. Rep. Online*, 2009, **65**, 184–185.
38 X. Wang, X. Wu, Y. Guo, Y. Zhong, X. Cao, Y. Ma and J. Yao, *Adv. Funct. Mater.*, 2010, **20**, 1680–1686.
39 P. Xing, D. Wu, J. Chen, J. Song, C. Mao, Y. Gao and H. Niu, *Analyst*, 2019, **144**, 2656–2661.
40 F. Y. Yi, J. P. Li, D. Wu and Z. M. Sun, *Chem.–Eur. J.*, 2015, **21**, 11475–11482.
41 J. Wang, Q. Zha, G. Qin and Y. Ni, *Talanta*, 2020, **211**, 120742.
42 X. Wang and C. Deng, *Talanta*, 2015, **144**, 1329–1335.
43 Y. Z. Li, G. D. Wang, Y. K. Lu, L. Hou, Y. Y. Wang and Z. Zhu, *Inorg. Chem.*, 2020, **59**, 15302–15311.
44 O. Filippou, E. A. Deliyanni and V. F. Samanidou, *J. Chromatogr. A*, 2017, **1479**, 20–31.
45 A. Li, K. Shen and J. Chen, *Chem. Eng. Sci.*, 2017, **166**, 66–76.
46 S. Li, D. Yang and F. Chen, *Int. J. Environ. Anal. Chem.*, 2017, **97**, 124–133.
47 G. D. Wang, Y. Z. Li, W. J. Shi, B. Zhang, L. Hou and Y. Y. Wang, *Sens. Actuators, B*, 2021, **331**, 129377.
48 Q. Wang, J. Yang, D. Zhang and L. Zhang, *J. Appl. Electrochem.*, 2016, **46**, 963–974.
49 Z. W. Zhai, S. H. Yang, M. Cao, L. K. Li, C. X. Du and S. Q. Zang, *Cryst. Growth Des.*, 2018, **18**, 7173–7182.
50 G. Qin, L. Li, W. Bai, Z. Liu, F. Yuan and Y. Ni, *Dyes Pigm.*, 2021, **190**, 109309.
51 J. Wang, Q. Zha, G. Qin and Y. Ni, *Talanta*, 2020, **211**, 120742.
52 J. R. Lakowicz, *Principles of fluorescence spectroscopy*, Springer, New York, 2006, p. 954.
53 W. Zhai, C. Wang, P. Yu, Y. Wang and L. Mao, *Anal. Chem.*, 2014, **86**, 12206–12213.
54 M. Lin, H. Y. Zou, T. Yang, Z. X. Liu, H. Liu and C. Z. Huang, *Nanoscale*, 2016, **8**, 2999–3007.
55 H. Cao, W. Dong, T. Wang, W. Shi, C. Fu and Y. Wu, *ACS Sustainable Chem. Eng.*, 2020, **8**, 10939–10946.